Inorg. Chem. **2007**, *46*, 10996–11002

Green Coloration of Co-Doped ZnO Explained from Structural Refinement and Bond Considerations

M. Gaudon,* O. Toulemonde, and A. Demourgues

Bordeaux Institute of Condensed Matter Chemistry, ICMCB-CNRS, 87 avenue du Dr. Albert Schweitzer, 33608 Pessac, Cedex, France

Received June 13, 2007

ZnO doped with Co^{2+} has been prepared by a Pechini process and investigated in terms of crystallographic structure and UV–visible properties. We emphasize for the first time a splitting of the ZnO band gap in two "sub-band gaps" (never clearly mentioned until now) which is fully interpreted basing on the iono-covalent nature of the O–Zn bonds. An anticipative approach of the potential structure relaxations was discussed from exchanged effective charge per bond calculated with the purely ionic Brown and Altermatt model.

Introduction

There has been a great deal of interest in the physical properties of diluted magnetic semiconductors (DMS). Wide band-gap semiconductors as matrixes are the most promising systems.[1]

Among these DMS candidates, ZnO doped with a small amount of a transition metal has been highly investigated (see reviews),[2] in particular, doped with cobalt ions. Moreover, controversies also still exist on the diluted magnetic properties exhibited by the doped ZnO oxides; some authors[3] noticed on well-characterized materials that these oxides fail to show ferromagnetism behavior. Most of the studies concern the elaboration of thin films. However, stoichiometry and phase purity can be difficult to establish in thin film. Furthermore, it is difficult to extract the intrinsic properties for the anisotropy effects. That is why little work on bulk doped ZnO has been carried out. Until now, depending on the method of synthesis, controversies still exist on the distribution of the dopant (Co^{2+}) inside the host matrix; some authors propose a dopant segregation to form a cluster, and on the other hand, one can think about a statistical distribution of the dopant inside the zincite structure.

Moreover, the ZnO:Co is a well-known green pigment which is largely developed, but the reason for its green coloration remains unclear despite UV−vis optical spectroscopic investigations.[2−7] It is currently well accepted that cobalt dopants inside ZnO allow tuning the gap toward low

Table 1. Rietveld Refinement Results

undoped ZnO ($P6_3mc$)		$R_p = 3.31\%$		$R_{wp} = 3.24\%$		$R_{Bragg} = 2.58\%$
$a = 3.2511(1)$ Å $c = 5.2051(1)$ Å						
atom	site	x	y	z	B_{iso}	occupancy
Zn	2b	0.3333	0.6667	0	0.7(4)	1
O	2b	0.3333	0.6667	0.3826(2)	0.7(2)	1
ZnO:Co 0.2 mol % ($P6_3mc$)		$R_p = 3.34\%$		$R_{wp} = 3.27\%$		$R_{Bragg} = 2.67\%$
$a = 3.2509(1)$ Å $c = 5.2049(1)$ Å						
atom	site	x	y	z	B_{iso}	occupancy
Zn	2b	0.3333	0.6667	0	0.80(4)	1
O	2b	0.3333	0.6667	0.3826(2)	0.9(2)	1
ZnO:Co 8 mol % ($P6_3mc$)		$R_p = 4.00\%$		$R_{wp} = 4.37\%$		$R_{Bragg} = 3.15\%$
$a = 3.2525(1)$ Å $c = 5.2038(1)$ Å						
atom	site	x	y	z	B_{iso}	occupancy
Zn	2b	0.3333	0.6667	0	0.5(1)	1
O	2b	0.3333	0.6667	0.3815(4)	0.6(3)	1

* Corresponding author. E-mail: gaudon@icmcb-bordeaux.cnrs.fr.

(1) Prellier, W.; Fouchet, A.; Mercey, B. *J. Phys. Condens. Matter* **2003**, *15* (37), R1583−R1601. Pearton, S. J.; Heo, W. H.; Ivill, M.; Norton, D. P.; Steiner, T. *Semicond. Sci. Technol*. **2004**, *19*, 10. Fukumara, T.; Toyosaki, H.; Yamada, H. *Semicond. Sci. Technol*. **2005**, *20*, S103.
(2) Koidl, P. *Phys. Rev. B* **1977**, *15*, 2493−2499. Risbud, A. S.; Spaldin, N. A.; Chen, Z. Q.; Stemmer, S.; Seisland, R. *Phys. Rev. B* **2003**, *68*, 205202.
(3) Rao, C. N. R.; Deepak, F. L. *J. Mater. Chem.* **2005**, *15* (5), 573−578.
(4) Deka, S.; Joy, P. A. *Chem. Matter* **2004**, *16*, 1168. Deka, S.; Joy, P. A. *Solid State Commun.* **2005**, *134*, 665−669.
(5) Bouloudenine, M.; Viart, N.; Colis, S.; Dinia, A. *Chem. Phys. Lett*. **2004**, *397*, 73−76.
(6) Ekambaram, S. *J. Alloys Compd.* **2005**, *390*, L4−L6.
(7) Maensiri, S.; Sreesongmuang, J.; Thomas, C.; Klinkaewnarong, J. *J. Magn. Magn. Mater*. **2006**, *301*, 422.

10.1021/ic701157j CCC: $37.00
Published on Web 11/16/2007

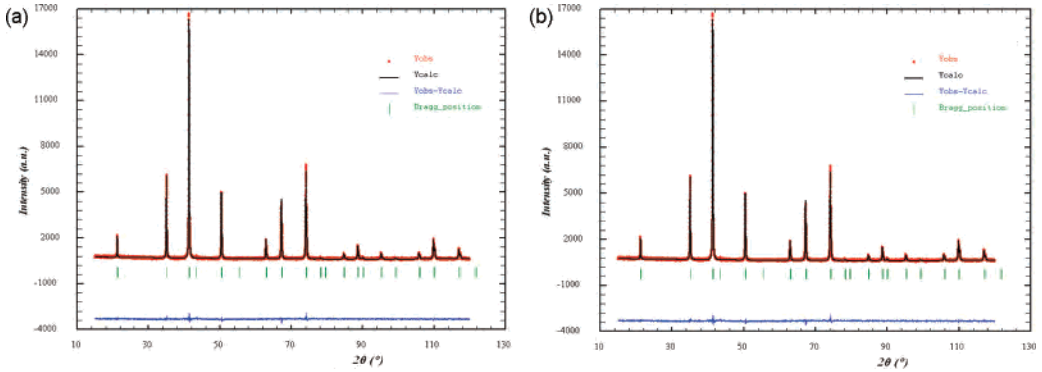

Figure 1. (a and b) Rietveld refinement plots for ZnO:Co 0.2 mol % and ZnO doped/Co 8 mol %, respectively.

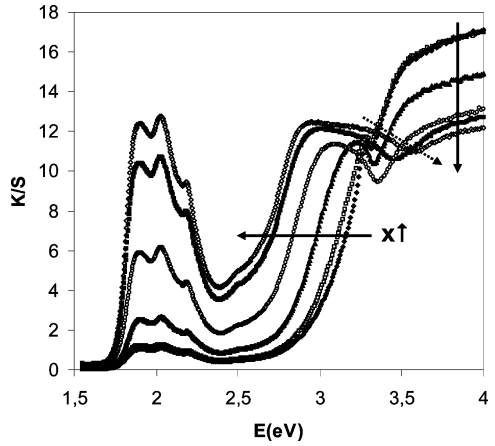

Figure 2. Kubelka−Munk absorption curves of Co-doped ZnO with x = 0.002, 0.005, 0.01, 0.02, 0.06, and 0.1.

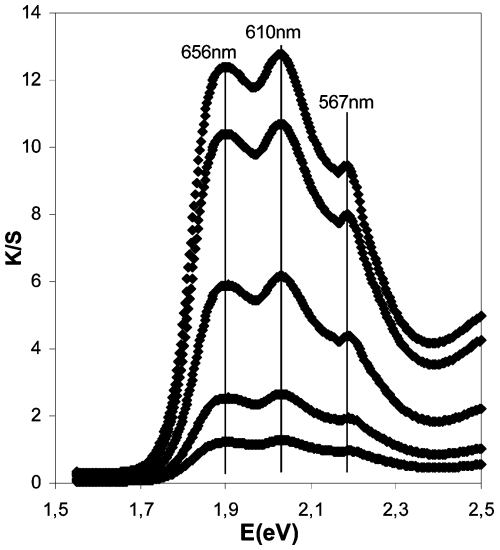

Figure 3. Kubelka−Munk absorption curves of Co-doped ZnO with x = 0.002, 0.005, 0.01, 0.02, 0.06, and 0.1. Zoomed in on the Co^{2+} d−d transitions.

energy, giving rise to the so-called red-shift phenomenon. This is explained by the authors by the strong exchange interaction between the d electrons of the doping ions with the sp carriers. Nevertheless, this red shift could be more easily explained by the dilatation of the oxygen−zinc bond lengths.[8] Indeed, it must be remembered that dilatation is the cause of the red shift observed for "all" semiconductor band gaps with increasing temperature: notably for ZnO, Bi_2O_3, In_2O_3, TiO_2, and V_2O_5, where the charge transfer occurs between a valence band mainly built with atomic orbitals of oxygen and a conduction band mainly built with the empty atomic orbitals of the metallic center. Since larger (Mn^{2+}) or smaller (Co^{2+}) cations than Zn^{2+} lead to the same band-gap red shift,[8] this second hypothesis based on cation size inducing internal pressure needs to be clarified. In this study, a new interpretation of the optical properties based on crystal structure relaxation around the doping cations is proposed for explaining ZnO band-gap modification with the cobalt for zinc substitution inside ZnO.

This article is focused on the ZnO gap modification with inserting cobalt ions in the structure. First, the crystallographic network was compared for undoped ZnO with literature results performed on the same composition synthesized using an equivalent low-temperature liquid route; then, in a second step, crystallographic modifications induced by Co doping were examined with X-ray diffraction techniques followed by Rietveld analyses. Moreover, the gap modification was followed with a UV−vis−NIR spectrometer equipped with an integration sphere. Finally, by correlating the two techniques it appears clearly that the band gap is not red shifted but split in two "other charge-transfer bands" while Co doping. This tendency has been explained by a clear and complete structural discussion based on the Brown and Altermatt valency calculations.[9]

Experimental Section

Synthesis Process. Co^{2+}-doped ZnO pigments were synthesized by the Pechini route (Pechini, N. U.S. Patent No. 3,330,697, 1967). This soft chemical process is based on cation chelation by citric acid (CA) and polyesterification between CA and ethylene glycol (EG), which leads to formation of a polycationic resin. Finally, oxides are obtained after heat treatment of this precursor resin at 1000 °C for 10 h under air.

Aqueous solutions of citrate were prepared by dissolving CA ($C_6H_8O_7 \cdot H_2O$; Sigma-Aldrich) in a minimal volume of water. Then cationic salts $Zn(NO_3)_2$, $6H_2O$, and $Co(NO)_3 \cdot 9H_2O$ (Aldrich) were added in stoichiometric proportion to the acid solution. A CA: cations molar ratio of 3:1 was used. After complete dissolution of metallic salts, EG ($C_2H_6O_2$; Sigma-Aldrich) was added to the mixture under magnetic stirring with a 4:1 EG:CA molar ratio. EG-

(8) Nassau, K. *The Physics of the Color*; John Wiley and Sons Inc.: London, 1983.

(9) Brown, I. D.; Altermatt, D. *Acta Crystallogr.* **1985**, *B41*, 244−247.

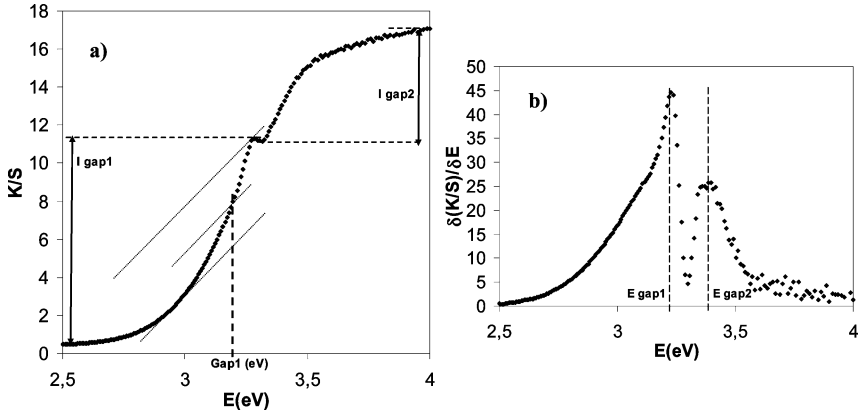

Figure 4. Kubelka−Munk absorption curves (a) and their first derivatives (b) of Co-doped ZnO with 0.2 mol %. Zoomed in on the two under band gaps.

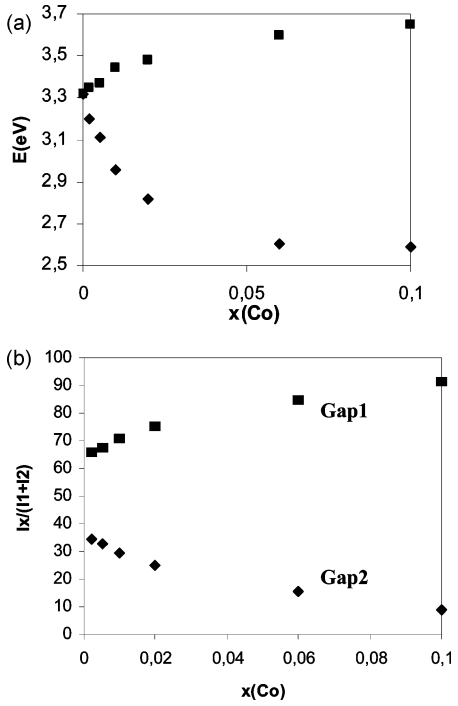

Figure 5. (a) Gaps energy versus *x* cobalt rate. (b) Gaps intensity ratio versus cobalt rate.

CA polymerization was promoted by removing water with continued heating over a couple of hours on a hot plate until solutions became highly viscous.

X-ray Powder Diffraction. A Philips PW 1820 apparatus equipped with a Cu($K\alpha_1$/$K\alpha_2$) source was used to evaluate the crystalline structure of all synthesized compounds. Diffraction patterns were collected with a 2θ step of 0.02° with a counting time of 10 s per step in routine mode or, for more advanced structural investigations, with a 2θ step of 0.015° with a counting time over 200 s per step. Diffractograms have been refined with the Rietveld method[10] using the FULLPROF program package. Unit cell parameters, atomic positions, occupancies, and Debye−Weller factors were refined and presented here.

Diffuse Reflectance Measurements. UV−vis−NIR spectroscopies were carried out in diffuse reflectance mode on a VARIAN CARY 5000 spectrophotometer equipped with an integrating sphere coated with polytetrafluoroethylene (PTFE). Measurements were performed for wavelengths varying from 200 to 2000 nm. HALON was used as white reference. All diffuse spectra are represented after Kubelka−Munk treatment: $(1 - R^2)/2R$ versus energy (in eV) considering that particle sizes are about 5-fold the analyzed wavelength domain (400−1000 nm).

Results and Discussion

Structural Description of ZnO Host Matrix. ZnO phase adopts a hexagonal symmetry with the $P6_3mc$ (No.186) space group. In such a structure, cations occupy flattened tetrahedral sites along the *c* axis responsible for the cell distortion. The tetrahedral sites of Zn^{2+} are both corner shared in a 3D space; from a local point of view, each tetrahedral site adopts a C_{3v} point group. Tetrahedral sites being flattened, the equilateral face perpendicular to the *c* axis exhibits the most important area with the longest O−O lengths. This anionic cage configuration, with trigonal distortion, causes a bringing together of zinc cation and the anionic equilateral face which can be explained, in analogy with corundum structure, by the increase of the metal−oxygen interaction as the opposite of the decrease of the oxygen−oxygen and metal−metal ones. Thus, the first four zinc−oxygen distances (forming the cationic center tetrahedral sites) become nonequivalent and can be described as three "short bonds" linking the zinc center and the ligands of the equilateral face and one "long bond" parallel to the *c* axis. Moreover, it can be noticed that the structure description is commonly based on the zinc atom placed in the specific position 2b with $z_{Zn} = 0$; here, the zinc out of the tetrahedron center moves toward the ligands along the *c* axis. Thus, the metallic center displacement is traduced here by the shift of the z_O position from 0.375 (position predicted in the case of undistorted tetrahedral sites) to 0.3828(2).

A first refinement analysis was performed for future comparison on undoped ZnO composition. The Riveted results (cell parameters, oxygen position, and reliability factors) are joined in the top of Table 1. It has to be noticed here than the ZnO crystallographic parameters do not significantly differ from the literature results obtained on ZnO synthesized from an equivalent route.[11]

Structural Description of Co-Doped ZnO Materials. Rietveld refinement results of two extreme rates are shown on 0.2 mol % of cobalt and 8 mol % of cobalt inserted in a

(10) Rietveld, H. M. *Acta Crystallogr.* **1967**, *22*, 151−158. Rietveld, H. M. *J. Appl. Crystallogr.* **1969**, *2*, 65−72.

(11) Kim, Y.; Page, K.; Seshadri, R. *Appl. Phys. Lett.* **2007**, *90*, 101904.

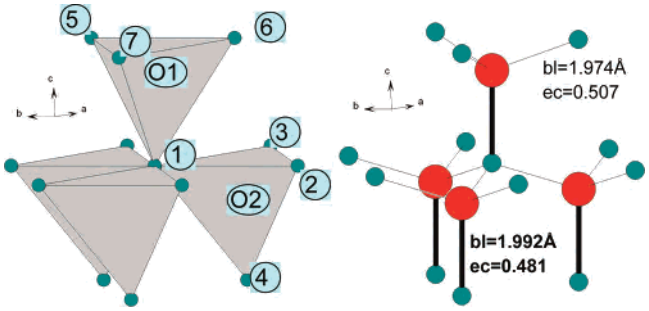

Figure 6. Characteristic cluster of a ZnO pure matrix, atoms indexation, bond lengths (bl), and corresponding exchanged charge (ce).

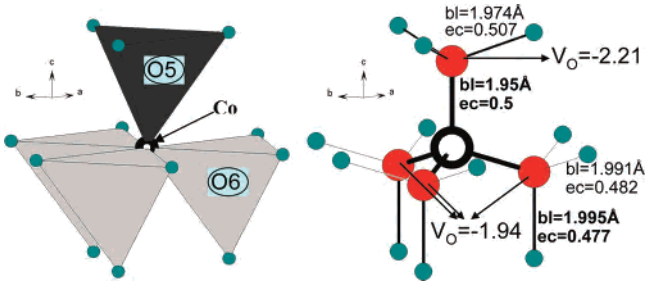

Figure 7. Characteristic cluster of a Co-doped ZnO, atoms indexation, bond lengths (bl), and corresponding exchanged charge (ec).

ZnO matrix. From a crystallographic point of view, the 0.2 mol % of cobalt-doped ZnO does not exhibit any difference with a pure ZnO elaborated under same conditions. For both contents a pure phase was obtained in the limit of X-ray detection. As illustrated, the experimental, calculated by the Rietveld method, and difference spectra are plotted in Figure 1a and b for the two doping rates. Results in terms of cell parameters and oxygen positions are presented in Table 1 for the 0.2 mol % and 8 mol % cobalt rates. Both results are in good agreement with the literature. First, the higher the cobalt rate, the higher the cell distortion, i.e., the *a* parameter increases whereas the *c* parameter decreases. Indeed, distortion degree, defined here as the ratio $R = (2a\sqrt{(2/3)})/c$ (thus, $R = 1$ represents no distortion), increases from 1.0198(1) for 0.2 mol % ZnO to 1.0207(2) for 8 mol % of cobalt in ZnO. An increase of the cell distortion degree is observed, whereas evolution of the z_O position tends to show that cobalt is placed in isotropic tetrahedral sites (in all cases, in a more isotropic tetrahedral site than zinc): indeed, z_O decreases from 0.3828 to 0.3815 for 0.2 mol % ZnO and 8 mol % doped ZnO, respectively. Thus, it can be of great interest to notice that X-ray diffraction analyses show clearly that the average tetrahedral sites of the transition metals are more "flattened" while cobalt ions are partially substituted for zinc ions. Nevertheless, it should be pointed out that the Co^{2+} cations are probably located in a more regular tetrahedral site than the zinc cations because notably of its electronic configuration ($e^4t_2^3$). The same kind of behavior has recently been published on $Zn_{1-x}Mg_xO$ ($0 \le x \le 0.15$) from X-ray synchrotron diffraction analyses.[11]

UV−vis Properties of Co-Doped ZnO Materials. For tetrahedral symmetry, with regard to Tanabe−Sugano diagrams established for a $3d^7$ electronic configuration, three transitions corresponding to ν_1 ($^4A_2(F) \rightarrow {}^4A_1(F)$), ν_2 ($^4A_2(F) \rightarrow {}^4T_1(F)$), and ν_3 ($^4A_2(F) \rightarrow {}^4T_1(P)$) are allowed.[12] For cobalt(II) ions the first two are known to be located in the infrared with a wavelength of about 1400 and 1600 nm, respectively. The third one is known to appear as a triplet due to the L−S Russel−Sanders coupling for which the maximal absorptions, for instance, in $CoAl_2O_4$ where the punctual symmetry of the tetrahedral site is T_d, are around 540, 590, and 640 nm.[12] This triple transition, centered in the orange region, leads to blue coloration when the material color is only due to the cobalt(II) ion located in a tetrahedral site as a unique chromophore.

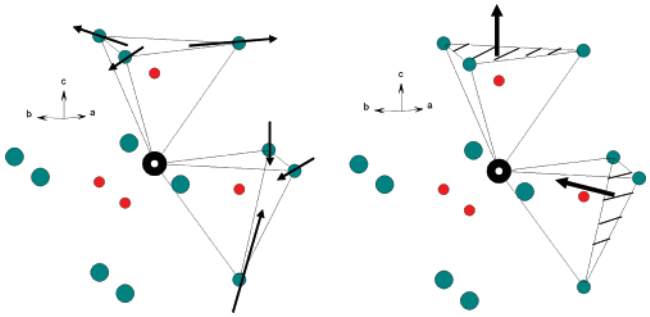

Figure 8. Two ways to get a constrain relaxation after Co doping.

Absorption properties of different cobalt-doped ZnO (for cobalt rate varying from 0.2 to 10 mol %) were recorded, and the Kubelka−Munk transformed curves are reported for energy varying in the range 1.5−4 eV in Figure 2.

On one hand, the reported diffuse reflectance spectra for the different cobalt rates clearly show that this triple transition characteristic of cobalt in a tetrahedral site is present whatever the cobalt rate studied. Furthermore, the positions of this triple transition, calculated from raw diffuse reflectance data, remain the same whatever the cobalt content at 567 (±2 nm depending on composition), 610 (±1 nm), and 656 nm (±1 nm) as it can be seen on the zoomed in K/S curves reported in Figure 3. The cobalt environment remains the same whatever the cobalt content; one can assume that cobalt adopts in all cases, at room temperature, its thermodynamically stable environment, i.e., as already assumed from X-ray diffraction analyses, cobalt is located in a nearly isotropic tetrahedral site.

On the other hand, the diffuse reflectance spectra show a splitting into two band gaps of the ZnO charge transfer shown in Figure 2 for 0.5 mol% composition. In literature, only the low-energy band gap was well characterized, leading the authors to the conclusion of a simple tuning of the ZnO band gap (red shift) with cobalt doping. The wavelength evolution of the two "sub-band gaps" detected here versus the cobalt rate and the intensity ratio ($I_{ratioX} = I_{gapx}/(I_{gap1} + I_{gap2})$) of these two gaps was extracted as shown in Figure 4 and reported in Figure 5a and b, respectively. From Figure 5a it can be seen that the two band gaps evolve in an opposite direction in terms of energy, the splitting being more and more pronounced versus the cobalt rate and tending to an asymptotic dwell. From Figure 5b it can be seen that the

(12) Llusar, M.; Forés, A.; Badenes, J. A.; Calbo, J.; Tena, M. A; Monrós, G. *J. Eur. Ceram. Soc.* **2001**, *21*, 1121−1130.

Table 2. Atom Positions and Bond Lengths Calculation of the Different Oxygen-center Tetrahedron Indexed in the Following Figures

pure ZnO host matrix	x	y	z	*x*(cor)	*y*(cor)	*z*(cor)	O1 tetrahedron	O2 tetrahedron
Zn1	0.000	1.877	0.000	0.000	0.000	−1.992	1.992	1.974
Zn2	1.625	−0.93 8	0.000	1.626	−2.815	−1.992		1.974
Zn3	3.251	1.877	0.000	3.251	0.000	−1.992		1.974
Zn4	1.625	0.938	−2.603	1.626	−0.939	−4.595		1.992
Zn5	−1.626	0.938	2.603	−1.626	−0.939	0.611	1.974	
Zn6	1.625	0.938	2.603	1.626	−0.939	0.611	1.974	
Zn7	0.000	3.754	2.603	0.000	1.877	0.611	1.974	
O1	0.000	1.877	1.992	0.000	0.000	0.000		
O2	1.625	0.938	−0.610	1.626	−0.939	−2.602		
theoretical $P6_3mc$ CoO	x	y	z	*x*(cor)	*y*(cor)	*z*(cor)	O3 tetrahedron	O4 tetrahedron
Co1	0.000	1.839	0.000	0.000	0.000	−1.950	1.950	1.950
Co2	1.592	−0.919	0.000	1.593	−2.758	−1.950		1.950
Co3	3.185	1.839	0.000	3.185	0.000	−1.950		1.950
Co4	1.592	0.919	−2.600	1.593	−0.920	−4.550		1.950
Co5	−1.593	0.919	2.600	−1.593	−0.920	0.650	1.950	
Co6	1.592	0.919	2.600	1.593	−0.920	0.650	1.950	
Co7	0.000	3.678	2.600	0.000	1.839	0.650	1.950	
O3	0.000	1.839	1.950	0.000	0.000	0.000		
O4	1.592	0.919	−0.650	1.593	−0.920	−2.600		
Co-doped ZnO	x	y	z	*x*(cor)	*y*(cor)	*z*(cor)	O5 tetrahedron	O6 tetrahedron
Co1	0.000	1.839	0.000	0.000	0.000	−1.950	1.950	1.950
Zn2	1.625	−0.938	0.000	1.626	−2.815	−1.992		1.991
Zn3	3.251	1.877	0.000	3.251	0.000	−1.99 2		1.991
Zn4	1.625	0.938	−2.603	1.626	−0.939	−4.595		1.995
Zn5	−1.626	0.938	2.603	−1.626	−0.939	0.611	1.974	
Zn6	1.625	0.938	2.603	1.626	−0.939	0.611	1.974	
Zn7	0.000	3.754	2.603	0.000	1.877	0.611	1.974	
O5	0.000	1.839	1.950	0.000	0.000	0.000		
O6	1.592	0.919	−0.650	1.593	−0.920	−2.600		

intensity of the high-energy band gap disappeared progressively to the benefit of the low-energy one.

Discussion

The ionic radius of Co^{2+} is smaller than that of Zn^{2+}: from Brown and Altermatt low's, in a tetrahedral site with oxygen at vertices, the cobalt−oxygen average bond length should be roughly 1.95 Å while the bond lengths in ZnO are 1.973 Å × 3 and 1.992 Å (values extracted from the ZnO:Co doped with 0.2 mol % refinement and corresponding also to the literature).[11,12] As indicated from the optical signature of Co^{2+}, one can consider, in a first approximation, the cobalt to adopt a T_d local environment (nearly isotropic tetrahedral site). Thus, with respect to Co−O bond lengths and considering purely isotropic tetrahedral Co sites, a "calculated" CoO oxide adopting a pure Wurtzite-type structure can be built: *a* and *c* parameters equal, respectively, to 3.185 and 5.200 Å have been found considering a regular tetrahedron ($z_O = 0.375$)—Diamond software has been used for checking this geometrical calculation. It is important to note here that the height of an isotropic cobalt tetrahedron (equal to one-half the *c* parameter, 2.600 Å) is calculated to be roughly equal to the height of a zinc tetrahedron (2.6025 Å), whereas the edge of the equilateral face of the tetrahedral site (001 face) is significantly shorter in the Co tetrahedron than in the Zn tetrahedron (3.185 instead of 3.2505 Å).

Following Vegard's law, from the linear combination of cell parameters of ZnO and the theoretical "zincite" CoO, the *a* parameter should strongly decrease while the *c* parameter remains stable. In fact, the cell parameters obtained from X-ray diffraction refinements show that *a* increases while *c* decreases. Nevertheless, the evolution of the *z* oxygen position versus the Co-doping rate is in good agreement with the hypothesis of an isotropic Co tetrahedron (associated with less and less oxygen decentring, only the oxygen position being a variable).

At this stage it was decided to investigate in more detail the structural impact of doping by a small and isotropic Co^{2+} cation.

The previous calculations showing a great difference between cobalt-center and zinc-center tetrahedral sites but the same tetrahedral sites height along the *c* axis underlines that the constrains occurring by Co doping should depend on the cell axis, leading to different relaxations or atomic reorganization according to the space directions. As shown in Figures 6and 7 in ZnO a zinc atom affects 12 zinc first-neighbors forming four oxygen-center tetrahedral sites. This figure also reports each bond length: "*bl*" as well as the "percentage of ionicity" (or effective charge, "ec") for each bond after calculation from the Brown and Altermatt valence model.[11] Furthermore, because the four oxygen-center tetrahedral sites are equivalent, values are reported only on one site. The longest oxygen−zinc bond, along the *c* axis, is clearly more covalent than the other ones. In Figure 8, in the same manner, the new situation obtained is represented, before any relaxation, after substitution of the central zinc tetrahedron by an isotropic cobalt-center tetrahedron following the values of Table 2.

For each bond length or effective charge calculations each atomic coordinate was transformed in Cartesian coordinates

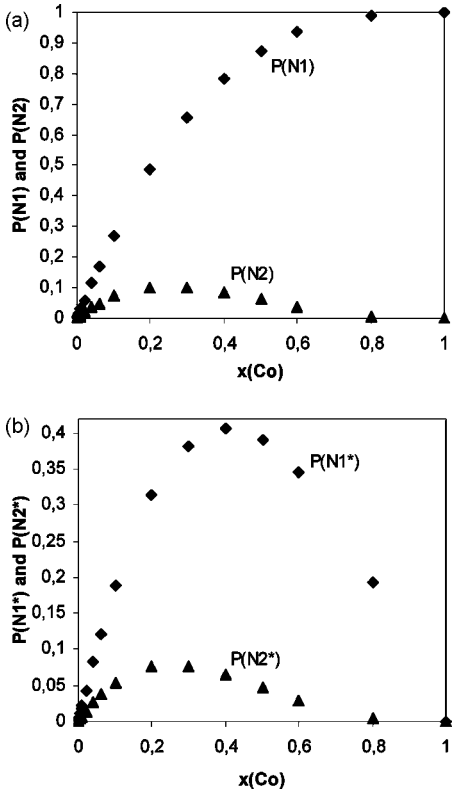

Figure 9. P(N1), P(N2), P(N1*), and P(N2*) probabilities versus cobalt rate.

(x, y, z). All results are summarized in Table 2. In the Co-doped ZnO, around the inserted cobalt (doping cation), the previously four equivalent oxygen-center tetrahedral sites can be decomposed here into three equivalent sites with light gray faces and a nonequivalent one with faces materialized in dark gray. As previously performed for Figure 6, nonequivalent atomic positions, bond lengths, and bond "percentage of ionicity" are reported in Figure 7. For the three equivalent oxygen-center tetrahedral sites, which could be "normally" predicted only considering a dilatation effect caused by substitution of zinc by a smaller ion, a decrease of the absolute value of the total valence (i.e., effective charge) of the first-neighbors oxygen anions (the valence is calculated here to be -1.94 instead of -2) is exhibited. For these tetrahedra two methods of relaxation can be considered for recovering the normal oxygen valency value. First, a reduction of the triangular face areas of the three "O6" tetrahedral sites located opposite the cobalt ion (reported on Figure 8 as the i mechanism); second, a shift of this triangular face toward the O6 anions (ii). Considering that several neighboring spheres would contribute to the constrains relaxation or considering a partial relaxation, the valence value of the central oxygen would remain a little bit less than 2 and a decrease in energy of the associated charge transfer of one electron from this anion to the Zn^{2+} ions forming this tetrahedral site would be observed, i.e., the band gap is red shifted. Indeed, an increase of the bond covalency is assumed here, leading to a decrease of the charge-transfer energy associated as explained in the Introduction. For the last tetrahedral site ("O5" one), the nonequivalent one, the valence value of the central oxygen anion becomes inferior

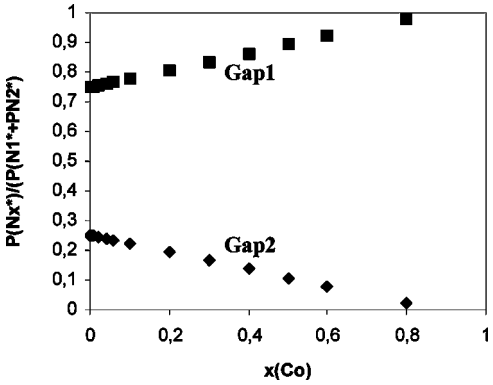

Figure 10. P(Nx*)/(P(N1*) + P(N2*)) probabilities ratio.

to -2. This reduction of the tetrahedral dimension leading to a decrease of the central anion valency is surprising only considering the Co^{2+} ionic size which is smaller than the Zn^{2+} one. For the same reasons as previously mentioned, relaxation can be envisaged first as an increase of the triangular face area opposite the cobalt(II) ion (iii) and second, the move away from "O5" of the Zn_3 triangular face toward the c direction (iiii). An increase in the energy of the band gap associated with this oxygen tetrahedron can be consequently predicted. Let us remember that X-ray diffraction shows the cell distortion increase versus cobalt doping (the c parameter decreases and the a parameter increases), indicating that the relaxation seems to be due to reduction/expansion of the opposite Zn_3 triangular faces and not by faces shift toward the cobalt position which would produce an increase of the flattening of the tetrahedral sites (as illustrated by the first scheme of Figure 8 which combines the i and iii mechanisms).

Lastly, we tried to determine if the evolution of the intensity ratio and their energetic positions of the two subgaps are in contradiction or not with a statistical distribution of cobalt inside the ZnO matrix. From a statistical distribution, a binomial law can be considered and a probabilistic model could be proposed to explain the asymptotic evolutions of the two band gaps and the progressive disappearance of the second one (high-energy gap) in terms of the intensity to the detriment of the first one (low-energy gap). It gives the probability of an oxygen tetrahedron to be dilated or contracted, i.e., associated to a band gap red or blue shift.

The probability for an oxygen to be directly in contact with k zinc cations and $n - k$ cobalt cations (here $n = 4$, the number of first-neighbor cations) corresponds to the probability of the binomial law $P(x = k) = (n!/(n - k)!k!)p^k q^{n-k}$, with q being the cobalt fraction and p the zinc one. Thus, it is easy to calculate the probabilities $P(0)$, $P(1)$, $P(2)$, $P(3)$, and $P(4)$ for different cobalt rates, ensuring the sum is equal to 1. It was considered, in agreement with the previously established hypothesis, that cobalt substitution for zinc in place 1, 2, or 3 (reporting to the O2 tetrahedron) leads to an expansion effect of the considered oxygen-center tetrahedron associated with the band gap red shift. However, substitution for zinc in place 4 leads to a contraction effect associated with the blue shift. Furthermore, it should be pointed out that if the two band-gap effects are present, the dilatation

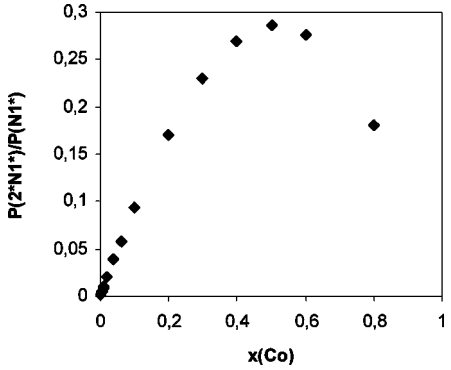

Figure 11. $P(2{\cdot}N1^*)/P(N1^*)$ probabilities ratio.

effect is the major one and so a red shift is macroscopically observed; it is consistent for cobalt and zinc ionic radii, Co^{2+} being smaller than Zn^{2+}, that the dilatation of the neighboring zinc tetrahedral sites is favored. Nevertheless, a more accurate model based on a DFT calculation would give probably a better view of the complex relaxation phenomenon linked to two antagonist effects.

Then the probability to get a dilated oxygen-center tetrahedron (red-shift source) was called $P(N1)$ and the probability to get a contracted oxygen tetrahedron called $P(N2)$. When one cobalt ion is inserted referred to ($P3$) probability, one-fourth of the four position (the 1 position) leads to a contraction phenomena, and when more than one cobalt ion is inserted, $P(2)$, $P(1)$, or $P(0)$ probabilities, a dilatation effect is in all cases induced since a dilatation plus a contraction antagonist phenomena leads to a global dilatation effect. Consequently, $P(N1) = 3/4P(3) + P(2) + P(1) + P(0)$ and $P(N2) = 1/4P(3)$, which are plotted in Figure 9a. One can also define the effective probability to get a red shift, i.e., the probability to transfer oxygen−zinc in a dilated tetrahedral, as $P(N1^*) = 3/4P(3){\cdot}3/4P(2){\cdot}1/2 + P(1){\cdot}1/4$, and in a same manner, one can define the effective probability to get a blue shift: $P(N2^*) = 1/4{\cdot}P(3){\cdot}3/4$; both are plotted in Figure 9b (only 3/4 of the tetrahedron bonds are $O^{2-}-Zn^{2+}$ ones when one Co^{2+} is inserted, only 2/4 bonds of the tetrahedron bonds are $O^{2-}-Zn^{2+}$ when two Co^{2+} are inserted, etc.). Note that $P(N1^*) + P(N2^*) + P(4) = p$, which traduces the total probability for a bond to be an oxygen−zinc bond. The ratios $P(Nx^*)/(PN1^* + PN2^*)$ (Figure 10) represent the probability for an $O^{2-}-Zn^{2+}$ bond to be dilated (N1*) or contracted (N2*) in the case where a bond modification is observed. The evolution of these ratios can be correlated with the evolution of the two band-gap intensity ratios. Indeed, our model predicts the disappearance of the blue-shifted band gap to the benefit of the red-shifted one. Nevertheless, the evolution is more rapid (gradient of the curve is more important) for the experimental curve than for the model prediction one. However, the asymptotic value as well as the starting ratio (for $x = 0$) are quite the same for the model and the experiment. Elsewhere it is possible to calculate the probability to get a strong expansion of the oxygen-center tetrahedron because of the presence of, at least, two cobalt atoms located at the corner positions 1, 2, or 3 (Figure 7): $P(2{\cdot}N1^*) = P(2){\cdot}1/2 + P(1){\cdot}1/4$. The probability ratio $P(2{\cdot}N1^*)/P(N1^*)$ (Figure 11), for a moderate cobalt rate, is an increasing function which can be correlated to the band-gap 1 evolution. Indeed, the band-gap 1 red shift with the cobalt rate can be interpreted as an increase of the average expansion of the dilated tetrahedral sites caused by the increase of the probability to find a "double" or "triple" expansion effect.

Conclusion

For $Zn_{1-x}Co_xO$ ($0 \le x \le 0.1$) X-ray diffraction studies have shown an increase of the oxygen position along the z axis associated with an increase of the cell distortion versus cobalt content x. This result can be explained considering cobalt cations are inserted on the ZnO matrix at the same crystallographic position as the zinc cations but in an isotropic tetrahedron, which is consistent with the triple intra-atomic absorption band curves, which evidence that cobalt is in a T_d environment whatever x and the spherical electronic configuration of Co^{2+} ions in T_d sites ($e^4t_2^3$). At the neighboring cobalt atoms inside the ZnO matrix, depending on their position besides the inserted cobalt atoms, two antagonist phenomena, explaining the observed optical band gap splits into two sub-band gaps, occur at the same time: the increase of some O−Zn bond lengths giving red-shift sources and the decrease of other O−Zn bond lengths giving blue-shift sources. The evolution in terms of the energy and intensity of these two sub-band gaps with cobalt doping is interpreted thanks to a statistical distribution of cobalt inside the ZnO matrix using a phenomenological model, giving the probability of an oxygen tetrahedron to be dilated or contracted, i.e., associated to a band-gap red or blue shift. The increase of the split width versus cobalt rate can be seen as a reinforcement of the expansion/contraction effect among the elongated/shortened O−Zn bonds with the cobalt rate; the disappearance of the high-energy subgap to the benefit of the low-energy one is due to a resultant dilating term when two opposite effects (dilatation and contraction) act at the same time on a O−Zn bond, consistent with the small ionic Co^{2+} radii in comparison to the Zn^{2+} one.

IC701157J